

Atomic layer deposition on gram quantities of multi-walled carbon nanotubes

This article has been downloaded from IOPscience. Please scroll down to see the full text article.

2009 Nanotechnology 20 255602

(<http://iopscience.iop.org/0957-4484/20/25/255602>)

[The Table of Contents](#) and [more related content](#) is available

Download details:

IP Address: 198.11.27.129

The article was downloaded on 03/06/2009 at 15:32

Please note that [terms and conditions apply](#).

Report Documentation Page

Form Approved
OMB No. 0704-0188

Public reporting burden for the collection of information is estimated to average 1 hour per response, including the time for reviewing instructions, searching existing data sources, gathering and maintaining the data needed, and completing and reviewing the collection of information. Send comments regarding this burden estimate or any other aspect of this collection of information, including suggestions for reducing this burden, to Washington Headquarters Services, Directorate for Information Operations and Reports, 1215 Jefferson Davis Highway, Suite 1204, Arlington VA 22202-4302. Respondents should be aware that notwithstanding any other provision of law, no person shall be subject to a penalty for failing to comply with a collection of information if it does not display a currently valid OMB control number.

1. REPORT DATE MAY 2009	2. REPORT TYPE	3. DATES COVERED 00-00-2009 to 00-00-2009	
4. TITLE AND SUBTITLE Atomic layer deposition on gram quantities of multi-walled carbon nanotubes		5a. CONTRACT NUMBER	
		5b. GRANT NUMBER	
		5c. PROGRAM ELEMENT NUMBER	
6. AUTHOR(S)		5d. PROJECT NUMBER	
		5e. TASK NUMBER	
		5f. WORK UNIT NUMBER	
7. PERFORMING ORGANIZATION NAME(S) AND ADDRESS(ES) University of Colorado, Department of Chemistry and Biochemistry, Boulder, CO, 80309		8. PERFORMING ORGANIZATION REPORT NUMBER	
9. SPONSORING/MONITORING AGENCY NAME(S) AND ADDRESS(ES)		10. SPONSOR/MONITOR'S ACRONYM(S)	
		11. SPONSOR/MONITOR'S REPORT NUMBER(S)	
12. DISTRIBUTION/AVAILABILITY STATEMENT Approved for public release; distribution unlimited			
13. SUPPLEMENTARY NOTES			
14. ABSTRACT Atomic layer deposition (ALD) was employed to grow coaxial thin films of Al₂O₃ and Al₂O₃/W bilayers on multi-walled carbon nanotubes (MWCNTs). Although the MWCNTs have an extremely high surface area, a rotary ALD reactor was successfully employed to perform ALD on gram quantities of MWCNTs. The uncoated and ALD-coated MWCNTs were characterized with transmission electron microscopy and x-ray photoelectron spectroscopy. Al₂O₃ ALD on untreated MWCNTs was characterized by nucleation difficulties that resulted in the growth of isolated Al₂O₃ nanospheres on the MWCNT surface. The formation of a physisorbed NO₂ monolayer provided an adhesion layer for the nucleation and growth of Al₂O₃ ALD films. The NO₂ monolayer facilitated the growth of extremely conformal coaxial Al₂O₃ ALD coatings on the MWCNTs. Cracks were also observed in the coaxial Al₂O₃ ALD films on the MWCNTs. After cracking, the coaxial Al₂O₃ ALD films were observed to slide on the surface of the MWCNTs and expose regions of bare MWCNTs. The Al₂O₃ ALD film also served as a seed layer for the growth of W ALD on the MWCNTs. The W ALD films can significantly reduce the resistance of the W/Al₂O₃/MWCNT wire. The results demonstrate the potential for ALD films to tune the properties of gram quantities of very high surface area MWCNTs.			
15. SUBJECT TERMS			
16. SECURITY CLASSIFICATION OF:			17. LIMITATION OF ABSTRACT Same as Report (SAR)
a. REPORT unclassified	b. ABSTRACT unclassified	c. THIS PAGE unclassified	
			18. NUMBER OF PAGES 11
			19a. NAME OF RESPONSIBLE PERSON

Atomic layer deposition on gram quantities of multi-walled carbon nanotubes

Andrew S Cavanagh^{1,2}, Christopher A Wilson³, Alan W Weimer⁴
and Steven M George^{2,3,4}

¹ Department of Physics, University of Colorado, Boulder, CO 80309, USA

² DARPA Center for Integrated Micro/Nano-Electromechanical Transducers (iMINT),
University of Colorado, Boulder, CO 80309, USA

³ Department of Chemistry and Biochemistry, University of Colorado, Boulder, CO 80309,
USA

⁴ Department of Chemical and Biochemical Engineering, University of Colorado, Boulder,
CO 80309, USA

Received 6 March 2009, in final form 1 May 2009

Published 3 June 2009

Online at stacks.iop.org/Nano/20/255602

Abstract

Atomic layer deposition (ALD) was employed to grow coaxial thin films of Al₂O₃ and Al₂O₃/W bilayers on multi-walled carbon nanotubes (MWCNTs). Although the MWCNTs have an extremely high surface area, a rotary ALD reactor was successfully employed to perform ALD on gram quantities of MWCNTs. The uncoated and ALD-coated MWCNTs were characterized with transmission electron microscopy and x-ray photoelectron spectroscopy. Al₂O₃ ALD on untreated MWCNTs was characterized by nucleation difficulties that resulted in the growth of isolated Al₂O₃ nanospheres on the MWCNT surface. The formation of a physisorbed NO₂ monolayer provided an adhesion layer for the nucleation and growth of Al₂O₃ ALD films. The NO₂ monolayer facilitated the growth of extremely conformal coaxial Al₂O₃ ALD coatings on the MWCNTs. Cracks were also observed in the coaxial Al₂O₃ ALD films on the MWCNTs. After cracking, the coaxial Al₂O₃ ALD films were observed to slide on the surface of the MWCNTs and expose regions of bare MWCNTs. The Al₂O₃ ALD film also served as a seed layer for the growth of W ALD on the MWCNTs. The W ALD films can significantly reduce the resistance of the W/Al₂O₃/MWCNT wire. The results demonstrate the potential for ALD films to tune the properties of gram quantities of very high surface area MWCNTs.

(Some figures in this article are in colour only in the electronic version)

1. Introduction

Carbon nanotubes (CNTs) have exceptional properties including low electrical resistance [1, 2], high mechanical strength [3, 4] and high thermal conductivity [5, 6]. CNTs can be used as building blocks for the fabrication of nanodevices including chemical sensors [7] and field-effect transistors [8]. CNTs can also be employed for many purposes such as field-emission electron sources [9] and nanoprobe for scanning probe microscopy [10]. There are many other emerging applications for both individual CNTs and dispersions of CNTs in composite materials [11, 12]. Many of these applications require thin films deposited on the CNTs to insulate, protect or functionalize the CNTs.

Atomic layer deposition (ALD) methods are preferred to obtain conformal and controlled film deposition at the atomic level. ALD is based on sequential, self-limiting surface reactions [13, 14] and has been reported for many materials [15, 16]. ALD can be applied to CNTs because ALD has been demonstrated on very high aspect ratio structures [17] and nanoparticles [18]. Al₂O₃ ALD growth has been reported on individual single-walled carbon nanotubes (SWCNTs) [19, 20] and multi-walled carbon nanotubes (MWCNTs) [21, 22]. The nucleation of Al₂O₃ ALD was identified as a significant problem for ALD on SWCNT surfaces [19, 20]. Fortunately, a functionalization procedure based on the adsorption of NO₂ and trimethylaluminum (TMA)

has been shown to yield an adhesion layer on SWCNTs [20]. This adhesion layer facilitates the nucleation of Al₂O₃ ALD and produces very conformal Al₂O₃ ALD films using TMA and H₂O as the reactants [20].

ALD on CNTs has been developed for CNT nanotube transistors and logic gates [23]. ZrO₂ ALD has been employed to deposit high dielectric constant insulating layers on CNTs to fabricate field-effect transistors [23]. HfO₂ ALD on SWNTs has also been achieved to fabricate high performance thin-film transistors [24]. Nucleation difficulties for ZnO ALD on MWCNTs has been shown to lead to bead-shaped crystalline particles on the surface of the MWCNTs that enhance electron field emission [25]. In contrast, coaxial ZnO/Al₂O₃ heterostructures were fabricated on CNTs after depositing an Al₂O₃ adhesion layer on CNTs [26]. Vanadium oxide ALD has also been employed to fabricate gas sensors from CNTs [27].

Most of the previous applications for ALD on CNTs have been demonstrated using single CNTs. Single individual CNTs avoid the many difficulties that are encountered when attempting ALD on large quantities of CNTs. Gram quantities of CNTs have an extremely high surface area of 200–300 m² g⁻¹ and can be entangled to form CNT aggregates. ALD on large quantities of CNTs has the same problems as ALD on particles in particle beds. The CNTs must be agitated to enhance gas conductance of the ALD reactants to the individual CNTs. Likewise, the CNTs must be displaced relative to each other during ALD to prevent the CNTs from being glued together by the ALD film. Enhanced gas conductance and constant CNT motion in the bed of CNTs can be accomplished using fluidized bed reactors [28, 29] or rotary reactors [30, 31].

ALD on large quantities of CNTs would be useful for preparing CNTs for CNT/polymer composites. CNT/polymer composites should have high mechanical strength, high thermal conductivity and high electrical conductivity. Possible applications for these CNT/polymer composites include transparent conductive coatings, electromagnetic interference shielding and flexible electrostatic dissipation films. There are many previously reported examples of CNT/polymer composites [32–36]. However, dispersion of CNTs in the polymer composite is a difficulty and may limit the properties of the CNT/polymer composite. ALD on the CNTs may help to improve the dispersion and coupling of CNTs in polymers.

The inertness of the surface of the CNT is the cause for the insolubility of CNTs in water and organic solvents [37] and the lack of dispersion of CNTs in polymers. Covalent functionalization can enhance CNT solubility [37] and provide coupling between CNTs and polymers [36]. Unfortunately, covalent functionalization of the CNT surface damages the inherent properties of the CNT [38]. Surfactants can also noncovalently functionalize the surface of CNTs without perturbing the underlying CNT properties [39, 40]. However, covalent and noncovalent functionalization of CNTs both require wet chemical treatment. ALD can deposit ultrathin coatings on CNTs using gas phase procedures that will facilitate CNT dispersion without requiring a solution process.

In this paper, ALD on large quantities of high surface area MWCNTs is demonstrated using a rotary ALD reactor. The

nucleation of Al₂O₃ ALD on gram quantities of MWCNTs is achieved using NO₂ and TMA to form an adhesion layer. Without the NO₂ nucleation procedure, the Al₂O₃ ALD grew nanospheres on the MWCNT surface. With the NO₂ nucleation procedure, the Al₂O₃ ALD grew very conformally on the MWCNTs. The ALD-coated MWCNTs were examined using transmission electron microscopy (TEM) and x-ray photoelectron spectroscopy (XPS) versus the number of Al₂O₃ ALD reaction cycles. The Al₂O₃ ALD coating was also used as a foundation for the subsequent growth of W ALD films on the MWCNTs.

2. Experimental details

2.1. MWCNTs and rotary reactor

The MWCNTs used in these experiments were 7000 series MWCNTs from Nanocyl (Sambreville, Belgium). For the Al₂O₃ ALD and W ALD, trimethylaluminum (97%) and WF₆ were obtained from Sigma-Aldrich (St Louis, MO). HPLC grade H₂O was also from Sigma-Aldrich and was further purified by five cycles of freeze–pump–thaw. For the NO₂ nucleation treatment, commercial purity grade NO₂ (99.5%) was acquired from Airgas (Radnor, PA). The Si₂H₆ used for W ALD was from Voltaix Inc. (Branchburg, NJ).

The specific surface areas of MWCNTs are on the order of hundreds of m² g⁻¹ [41–43]. From Brunauer, Emmett and Teller (BET) measurements, the manufacturer reports a specific surface area of 250–300 m² g⁻¹ for the 7000 series MWCNTs. This surface area is approximately an order of magnitude larger than for the nanopowders previously coated with ALD [30]. For equivalent masses of material, larger reactant exposures and purge times are required for the MWCNTs compared with typical nanopowders. BET measurements may also probe the inner surfaces of the MWCNT if the MWCNTs have open ends.

ALD on particles is possible using either fluid bed reactors [28, 29] or rotary reactors [30, 31]. Rotary reactors have an advantage when performing ALD on nanoparticles because the rotary reactors can provide for static reactant exposures [30]. These static reactant exposures can minimize the amount of reactant that is lost to the vacuum pump. Recent work has demonstrated the feasibility of ALD on gram quantities of nanopowders in a rotary reactor [30]. The rotary reactor employed in this study was similar to the rotary reactor employed in the previous work [30, 31].

A schematic of the rotary reactor is shown in figure 1. Each reactant entered the reaction chamber (A) through a needle and pneumatic valves (B) that were attached to 0.25" welded ports on a custom 6.0" conflat cap (C). During the reaction, the MWCNTs were mechanically agitated in a rotating porous cylinder (D). The rotation was achieved via a magnetically coupled rotary feedthrough (E). The pressure was monitored with 10 and 1000 Torr capacitance manometers (F). A gate valve (G) was opened to exhaust product gases and any excess precursor to the pump (H).

Before coating the MWCNTs in the rotary reactor, MWCNT quantities from 20 mg to 2 g were placed in the

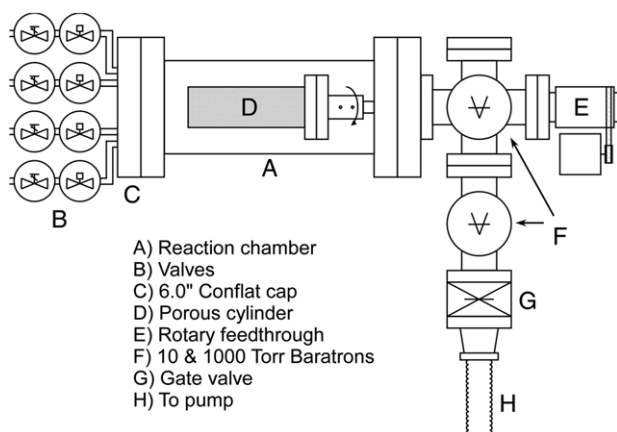


Figure 1. Schematic of rotary reactor used to coat gram quantities of MWCNTs.

porous stainless steel cylinder with a pore size of 10 μm . The porous metal cylinder was then attached to the magnetically coupled rotary feedthrough (E). This feedthrough with the porous metal cylinder was then enclosed in the vacuum chamber of the rotary reactor and left to outgas under vacuum for 24 h. Vacuum was obtained using a dual-stage rotary vane pump. Pressure was monitored with a Baratron capacitance manometer (MKS, Andover, MA). For the larger quantities of MWCNTs, the reactant exposures were scaled linearly according to the sample mass. For 1–2 g samples of MWCNTs, multiple doses of precursors were required to achieve the desired reactant exposure [31].

A ceramic heater (Watlow Electric Manufacturing Co., St Louis, MO) on the rotary reactor was employed for reactions performed at elevated temperatures. The temperature was monitored with a thermocouple and was manually controlled by applying a constant voltage to the resistive heating element. During the NO_2 functionalization treatment and ALD processing, the porous metal cylinder was rotated in the rotary reactor at ~ 150 rpm. Given the diameter of the rotating porous cylinder, this rotational frequency is consistent with a centripetal acceleration of ~ 0.5 g where g is gravitational acceleration. Reasonable results were obtained using rotational frequencies from 140–180 rpm. Rotational frequencies < 140 rpm led to less agitation and agglomeration during ALD. Rotational frequencies > 180 rpm led to agglomeration resulting from the CNTs staying on the walls of the porous cylinder.

2.2. Al_2O_3 ALD and surface nucleation chemistry

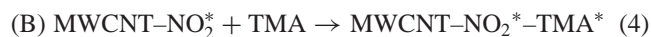
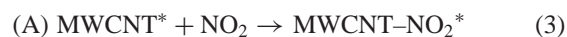
Al_2O_3 ALD was performed on gram quantities of MWCNTs in the rotary reactor. The Al_2O_3 ALD surface chemistry employs $\text{Al}(\text{CH}_3)_3$ (TMA) and H_2O as the reactants. The sequential, self-limiting reaction sequence during Al_2O_3 ALD is [44–46]:



where the asterisks denote surface species. The Al_2O_3 ALD reaction sequence was: (1) TMA dose to set pressure; (2) TMA

reaction time; (3) evacuation of reaction products and excess TMA; (4) N_2 dose; (5) N_2 static time; (6) evacuation of N_2 and any entrained gases; (7) H_2O dose to pressure; (8) H_2O reaction time; (9) evacuation of reaction products and excess H_2O ; (10) dose N_2 ; (11) N_2 static time; and (12) evacuation of N_2 and any entrained gases. This sequence constituted one AB cycle of Al_2O_3 ALD.

During the NO_2 nucleation treatment, an adsorbed functionalization layer was initially formed on the MWCNTs by alternating exposures of NO_2 and TMA [20]:



where the asterisks indicate surface species. In this functionalization process, the nitrogen of the NO_2 is attracted to the CNT surface and leaves the oxygen atoms accessible. Upon TMA exposure, the oxygen atoms coordinate to the aluminum of the TMA molecule leaving a methyl-terminated surface [20]. The methyl-terminated surface does not interact with subsequent NO_2 exposures.

Following the previous nucleation procedure [20], 50 cycles of NO_2 /TMA were used to functionalize the MWCNTs at room temperature. This NO_2 treatment was performed with the following sequence: (1) exposure to NO_2 to set pressure; (2) NO_2 static reaction time; (3) evacuation of excess NO_2 ; (4) exposure to TMA to set pressure; (5) TMA static reaction time; and (6) evacuation of excess TMA. This sequence defines one AB cycle of the NO_2 /TMA functionalization layer. For 20 mg of MWCNTs, the dose pressures were 300 mTorr for both NO_2 and TMA. The static reaction times for NO_2 and TMA were 10 s. The NO_2 and TMA purge times were 7 s and 30 s, respectively. The NO_2 /TMA functionalization layer will desorb at elevated temperatures. Consequently, the adsorbed NO_2 /TMA layer was stabilized with 5 AB cycles of Al_2O_3 ALD at room temperature. Al_2O_3 ALD growth could then be continued at higher reaction temperatures.

For the Al_2O_3 ALD on the untreated MWCNTs and on the NO_2 /TMA functionalized MWCNTs, the Al_2O_3 ALD reaction sequence was employed at 180 $^\circ\text{C}$. For 20 mg of MWCNTs, the dose pressures were 1.0 Torr for TMA and H_2O and 20 Torr for N_2 . The reaction times for the TMA and H_2O were both 60 s. The N_2 static time was 5 s. All purge times were 60 s. Figure 2 displays the ALD reactor pressure versus time for one AB cycle of Al_2O_3 ALD for (a) untreated MWCNTs and (b) NO_2 /TMA functionalized MWCNTs.

For both the untreated MWCNTs and the NO_2 /TMA functionalized MWCNTs, the pressure responses during the TMA doses shown in figures 2(a) and (b) are similar. The pressure responses during the H_2O doses were different for the untreated MWCNTs and NO_2 /TMA functionalized MWCNTs. For the untreated MWCNTs, figure 2(a) reveals that the pressure dropped following the H_2O dose of 1 Torr. For the NO_2 /TMA functionalized MWCNTs, figure 2(b) shows that the pressure dipped briefly and then returned to 1 Torr.

The difference in behavior for H_2O on the untreated MWCNTs and the NO_2 /TMA functionalized MWCNTs is accounted for by the difference in reactive surface areas. The

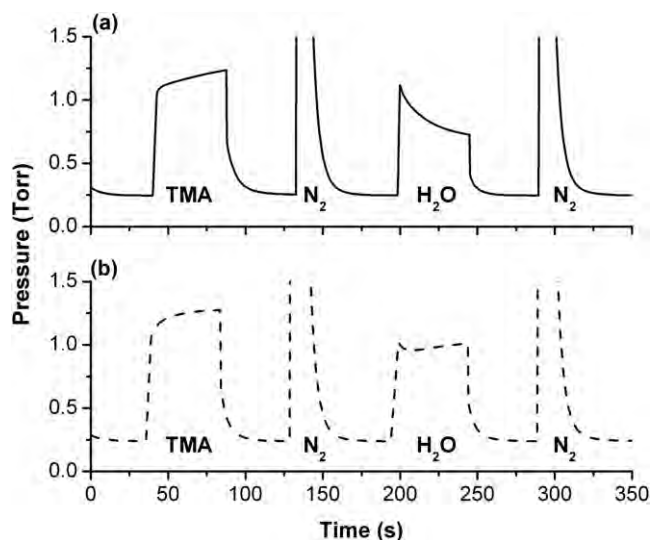
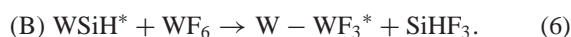
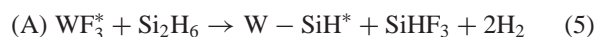


Figure 2. Reactor pressure versus time for one AB cycle during Al_2O_3 ALD for (a) untreated MWCNTs and (b) NO_2/TMA functionalized MWCNTs.

conformally coated MWCNTs have a larger Al_2O_3 surface area. The H_2O reacts nearly completely on this surface area and little extra H_2O is available for reabsorption. The pressure stays close to 1 Torr because H_2O is converted to CH_4 reaction product. For the untreated MWCNTs and an equivalent H_2O exposure, the growth of Al_2O_3 nanospheres only consumes a fraction of the H_2O . The excess H_2O molecules then slowly adsorb on the Al_2O_3 surface.

After depositing an Al_2O_3 ALD layer on the MWCNTs, other ALD coatings can be applied such as W ALD. W ALD was accomplished using WF_6 and Si_2H_6 as the reactants. The sequential, self-limiting reaction sequence for W ALD is [47, 48]



The W ALD chemistry is not a truly self-limiting process. W ALD is dependent on the Si_2H_6 exposure and the substrate temperature [49]. A typical growth rate for W ALD is $\sim 5 \text{ \AA}/\text{cycle}$ [50].

For W ALD on the MWCNTs, the W ALD reaction sequence was: (1) dose Si_2H_6 to set pressure; (2) Si_2H_6 reaction time; (3) evacuation of reaction products and excess Si_2H_6 ; (4) N_2 dose; (5) N_2 static time; (6) evacuation of N_2 and any entrained gases; (7) dose WF_6 to set pressure; (8) WF_6 reaction time; (9) evacuation of reaction products and excess WF_6 ; (10) dose N_2 ; (11) N_2 static time; and (12) evacuation of N_2 and any entrained gases. This sequence constituted one AB cycle of W ALD. The W ALD reaction sequence was employed at 180°C . For 20 mg of MWCNTs, the dose pressures were 1.0 Torr for the Si_2H_6 and WF_6 and 20 Torr for the N_2 . The reaction times for the Si_2H_6 and WF_6 were 200 s and the purge times were both 50 s. The N_2 static time was 20 s and the purge time was 200 s.

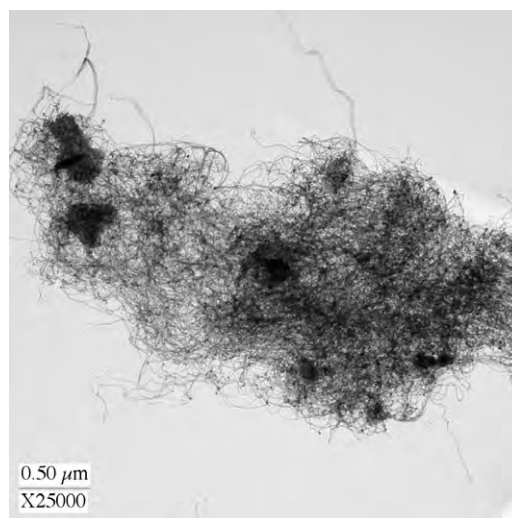


Figure 3. TEM image of an uncoated entangled cluster of MWCNTs.

2.3. TEM and XPS analysis

Transmission electron microscopy (TEM) images of the MWCNTs and ALD-coated MWCNTs were collected on a Philips CM10 electron microscope (Mahwah, NJ). A Gatan digital camera (Gatan, Pleasanton, CA) was used to record the images. Measurements of the micrographs were made in Deneba Canvas 9 (ACD Systems, Victoria, British Columbia, Canada). These measurements were used to determine the film thickness.

A PHI 5600 x-ray photoelectron spectrometer was used to obtain x-ray photoelectron spectra (XPS) of the ALD-coated MWCNTs. The powder samples were pressed into pellets with a thickness of 0.7 mm and a diameter of 5.5 mm and affixed to the sample puck with carbon tape. Monochromatic $\text{Al K}\alpha$ x-rays (1486.6 eV) were used for the XPS analysis. The pass energy was 58.7–93.9 eV and the step size was 0.250–0.400 eV. An electron beam neutralizer was employed at 17.8 mA. Data was collected with Auger Scan (RBD Enterprises, Inc., Bend, OR). XPS data was analyzed in CASA XPS (Casa Software Ltd, UK). Peak fits for the W 4f peaks were obtained using a linear background and a 70:30 Gaussian:Lorentzian peak.

3. Results and discussion

3.1. Entangled MWCNT clusters

Transmission electron microscopy (TEM) images were used to characterize the MWCNTs and the ALD film growth on the MWCNTs. The uncoated MWCNTs were a fine powder. These uncoated MWCNTs displayed a range of tube diameters as observed by TEM. The manufacturer reported an average tube diameter of 10 nm. The nanotubes were also agglomerated in entangled clusters prior to the ALD coating. A TEM image of these uncoated entangled clusters of MWCNTs is displayed in figure 3. The diameter of these entangled clusters was $\sim 2\text{--}3 \mu\text{m}$.

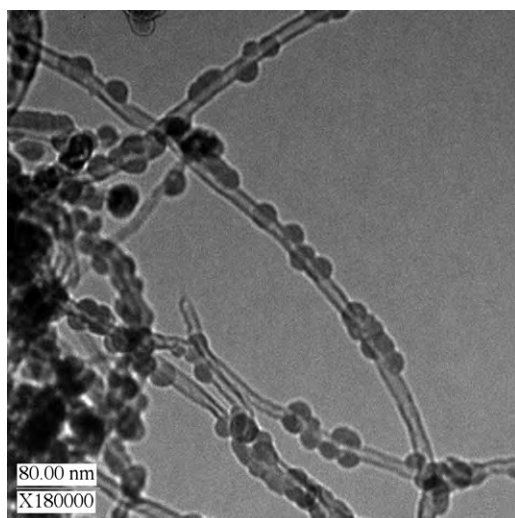


Figure 4. TEM image of untreated MWCNTs after 50 AB cycles of Al_2O_3 ALD.

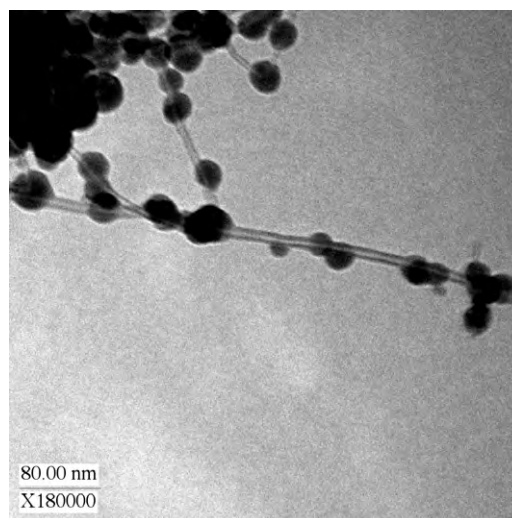


Figure 5. TEM image of untreated MWCNTs after 100 AB cycles of Al_2O_3 ALD.

TEM images of the coated MWCNTs were typically imaged on the edge of a μm -scale entangled cluster. Further agglomeration of the MWCNTs during ALD was prevented by performing the ALD in the rotary reactor under agitation by rotation [30]. There were still μm -scale agglomerates of MWCNTs after ALD processing. Some of these agglomerates were mechanically crushed prior to TEM analysis to obtain MWCNTs from the center of the entangled clusters. MWCNTs from the edge and center of the entangled clusters were all found to be coated with Al_2O_3 ALD.

3.2. Al_2O_3 ALD nanospheres on untreated MWCNTs

ALD Al_2O_3 on untreated MWCNTs resulted in the growth of Al_2O_3 nanospheres. A TEM micrograph of these nanospheres after 50 AB cycles is shown in figure 4. The nanospheres are fairly spherical and monodisperse. The radii of the nanospheres are in the range of 11–13 nm. The TEM images suggest that Al_2O_3 ALD growth nucleates at specific sites on the MWCNT surface during the initial Al_2O_3 ALD cycles. The nanospheres then grow isotropically versus the number of AB cycles to yield fairly monodisperse sphere diameters. Very similar Al_2O_3 nanospheres were observed earlier after Al_2O_3 ALD on individual SWCNTs [19].

Figure 5 shows TEM images of the Al_2O_3 nanospheres after 100 AB cycles. There is an increase in the nanosphere diameter and the number of nanospheres after 100 AB cycles. However, the nanospheres are not as monodisperse compared with the nanospheres after 50 ALD cycles. The radii of the nanospheres range from 11–20 nm. This finite range indicates that the Al_2O_3 ALD nanospheres do not all nucleate at the same time. Sites that nucleate later should experience fewer Al_2O_3 ALD cycles and produce nanospheres with smaller radii. For adjacent nanospheres, the spheres eventually begin to coalesce to form a rough, pseudo-continuous Al_2O_3 film.

Previous studies of Al_2O_3 ALD on individual MWCNTs have observed conformal growth on nanotube surfaces that were not intentionally functionalized [21, 22]. In contrast,

figures 4 and 5 reveal that the Al_2O_3 ALD growth was not conformal in this study. Distinct nanospheres are observed that are similar to the Al_2O_3 nanospheres observed after Al_2O_3 ALD on unfunctionalized SWCNTs [19]. A possible explanation for this difference in growth involves the presence of defects or inadvertent chemical functionalization on the earlier MWCNT surfaces.

The density of defects and chemical functional groups on the MWCNT surface may be related to the method of MWCNT synthesis and subsequent cleaning and purification methods [51]. The growth of nanospheres may be expected for a low density of defects or active chemical species on the MWCNT surface. If the density of defects or active chemical species is much higher, the larger density could lead to a conformal Al_2O_3 ALD film. The defect density may have been significantly lower for the MWCNTs utilized in this study compared with MWCNTs used in previous studies [21, 22].

3.3. Conformal Al_2O_3 ALD growth on NO_2 /TMA functionalized MWCNTs

To grow conformal Al_2O_3 ALD coatings on gram quantities of MWCNTs, a functionalization layer of adsorbed NO_2 and TMA was initially formed at room temperature. This adsorbed layer is not stable at the elevated temperatures typically used to grow Al_2O_3 ALD. However, this adsorbed layer can be stabilized with an Al_2O_3 passivation layer consisting of 5 AB cycles of Al_2O_3 ALD at room temperature. The Al_2O_3 ALD chemistry readily nucleated and grew conformally on this adsorbed layer.

Additional Al_2O_3 ALD cycles were performed at 180°C to achieve the desired Al_2O_3 ALD film thickness. Figure 6 displays a TEM image after 50 AB cycles of Al_2O_3 ALD on the NO_2 /TMA functionalized MWCNTs. In contrast to the nanospheres observed in figure 4 after 50 AB cycles, the Al_2O_3 films are smooth and conformal after 50 AB cycles on the NO_2 /TMA functionalized MWCNTs. A second TEM image showing a larger portion of the entangled MWCNT

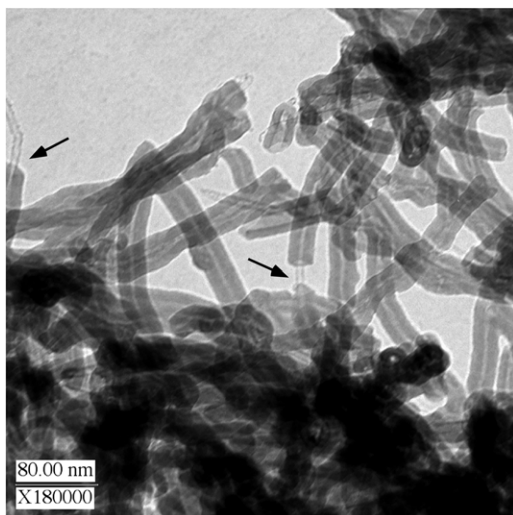


Figure 6. TEM image of NO₂/TMA functionalized MWCNTs after 50 AB cycles of Al₂O₃ ALD.

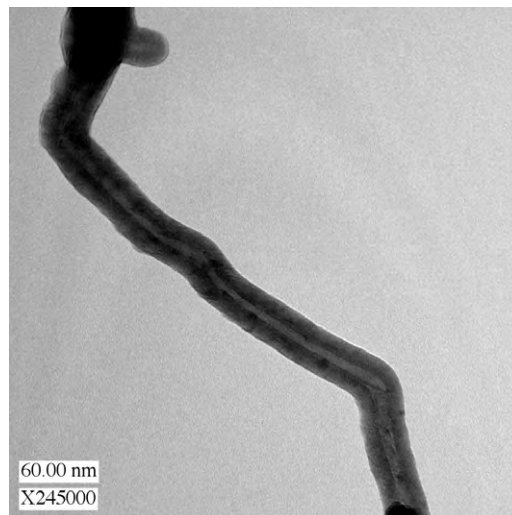


Figure 8. TEM image of NO₂/TMA functionalized MWCNTs after 40 AB cycles of Al₂O₃ ALD at higher magnification.

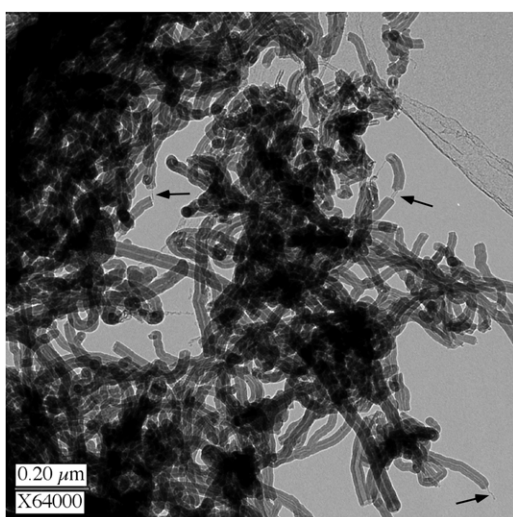


Figure 7. TEM image of NO₂/TMA functionalized MWCNTs after 50 AB cycles of Al₂O₃ ALD at lower magnification.

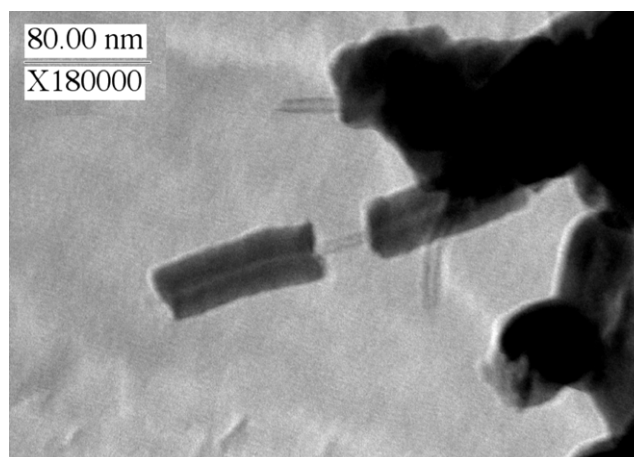


Figure 9. TEM image of NO₂/TMA functionalized MWCNTs after 60 AB cycles of Al₂O₃ ALD showing evidence for Al₂O₃ ALD film cracking and sliding on MWCNTs.

cluster at a reduced magnification is presented in figure 7. A conformal Al₂O₃ ALD coating is observed on all the MWCNTs.

Figure 8 shows an enlargement of a coated MWCNT after 40 AB cycles. The Al₂O₃ ALD film is extremely conformal on the MWCNT. TEM images were performed after 25, 40, 50 and 60 AB cycles. TEM analysis of the film thickness was consistent with Al₂O₃ ALD growth that was linear with the number of AB cycles. The Al₂O₃ ALD growth per cycle was 1.7 Å/cycle. This Al₂O₃ ALD growth per cycle is slightly larger than the growth per cycle of 1.1–1.2 Å/cycle reported for Al₂O₃ ALD on flat substrates [45, 46]. However, this Al₂O₃ ALD growth rate is in agreement with the growth rates reported for Al₂O₃ ALD on nanopowders of 1.8–2.0 Å/cycle [18, 30]. The larger growths per cycle may result from the inability to purge H₂O completely from very high surface area samples.

3.4. ‘Macaroni’ on MWCNT string

According to the proposed NO₂ nucleation mechanism, the Al₂O₃ ALD films are grown on an adsorbed layer of NO₂/TMA on the CNTs [20]. This adsorbed layer is not covalently attached to the surface of the CNT. Consequently, the coaxial Al₂O₃ ALD film on the CNTs should be free to slide along the CNTs. TEM images reveal this ‘sliding’ behavior. Locations where the Al₂O₃ ALD film has broken on the MWCNT show evidence for the sliding of the Al₂O₃ ALD film along the MWCNT. Broken Al₂O₃ ALD films that have moved to reveal bare MWCNTs are indicated by the arrows in figures 6 and 7.

These broken sections of coaxial Al₂O₃ ALD film on the MWCNT are like ‘macaroni’ on an MWCNT string. A TEM image that captures a segment of an Al₂O₃ ALD film on the MWCNT is displayed in figure 9. This Al₂O₃ ALD film was deposited using 60 AB cycles. The mechanical tumbling of the entangled clusters of MWCNTs may facilitate the breaking of the Al₂O₃ ALD films at the ends of MWCNTs. These Al₂O₃

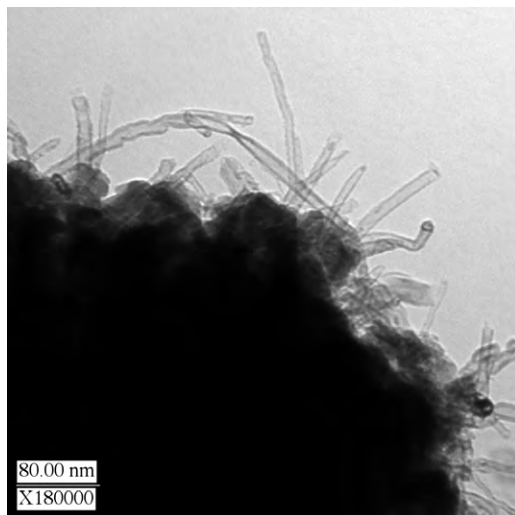


Figure 10. TEM image of NO₂/TMA functionalized MWCNTs after 60 AB cycles of Al₂O₃ ALD showing bare MWCNTs at the perimeter of the entangled MWCNTs. These bare MWCNTs result from the Al₂O₃ ALD film cracking and sliding off the MWCNTs.

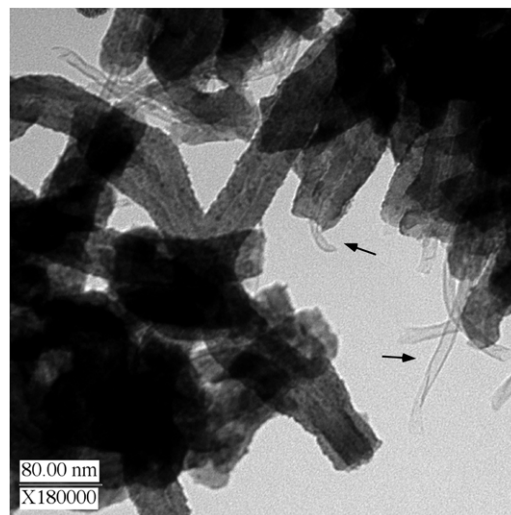


Figure 11. TEM image after 60 cycles of W ALD on Al₂O₃ surface prepared by NO₂/TMA functionalization and 50 AB cycles of Al₂O₃ ALD on MWCNTs.

ALD segments may then slide off the MWCNTs to reveal bare MWCNTs at the edge of an entangled cluster. Figure 10 shows a TEM image that reveals a number of bare MWCNTs dangling at the perimeter of an entangled MWCNT cluster.

3.5. Bilayers of W ALD/Al₂O₃ ALD on MWCNTs

The conformal coaxial Al₂O₃ ALD coating on MWCNTs can serve as a substrate for the subsequent growth of another ALD material. W ALD was performed on the Al₂O₃ ALD coating to deposit a W/Al₂O₃ bilayer on the MWCNTs. The initial Al₂O₃ ALD film was prepared using the NO₂/TMA nucleation procedure and then 50 cycles of Al₂O₃ ALD. Subsequently, W ALD was grown on the Al₂O₃ ALD surface. Figure 11 displays a TEM image after 60 cycles of W ALD using WF₆ and Si₂H₆. The W ALD leads to an increase in diameter of the coated MWCNTs. Bare MWCNTs where the W/Al₂O₃ bilayer has slipped off the ends of the MWCNTs are also indicated by the arrows.

The surface of the W/Al₂O₃ bilayer film is rougher and more granular than the Al₂O₃ ALD film on MWCNTs. The surface roughness may be caused by the polycrystal W ALD film or difficulties for the W ALD nucleating on the Al₂O₃ ALD surface [52–54]. Both of these factors are believed to affect the roughness of W ALD layers in W/Al₂O₃ nanolaminates [53, 55]. In spite of the increased roughness, the W/Al₂O₃ bilayer film is still conformal to the MWCNTs. TEM measurements of the W ALD film thickness were difficult because of the lack of a distinct boundary between the Al₂O₃ ALD film and the W ALD film. While the density disparity between Al₂O₃ ALD and W ALD should be evident, the geometry of the two coaxial nested cylinders prevented this distinction.

X-ray photoelectron spectroscopy (XPS) was used to analyze: (a) the uncoated MWCNTs; (b) the Al₂O₃ ALD on the untreated MWCNTs; (c) the Al₂O₃ ALD on the NO₂/TMA

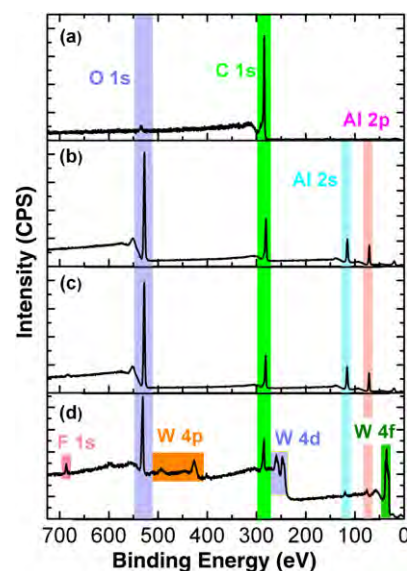


Figure 12. XPS scans of: (a) untreated MWCNTs; (b) untreated MWCNT after 100 AB cycles of Al₂O₃ ALD; (c) MWCNTs after NO₂/TMA functionalization and 100 AB cycles of Al₂O₃ ALD; and (d) MWCNTs after NO₂/TMA functionalization and 50 AB cycles of Al₂O₃ ALD and 60 AB cycles of W ALD.

functionalized MWCNTs; and (d) the W ALD on the Al₂O₃ ALD on the NO₂/TMA functionalized MWCNTs. The XPS spectrum of uncoated MWCNTs shown in figure 12(a) displayed a distinct C 1s peak with a full width at half-maximum (FWHM) of 1.5 eV. The XPS spectrum of Al₂O₃ ALD on untreated MWCNTs shown in figure 12(b) also displayed peaks for Al, C and O. All of these peaks had a broader FWHM of ~2.6 eV. This slight broadening may result from charging effects attributed to the presence of Al₂O₃ on the MWCNTs. The typical ratio for Al:O was 2:2.6 determined from the Al 2p and O 1s XPS signals.

The XPS spectrum of Al₂O₃ ALD on the NO₂/TMA functionalized MWCNTs is displayed in figure 12(c). The

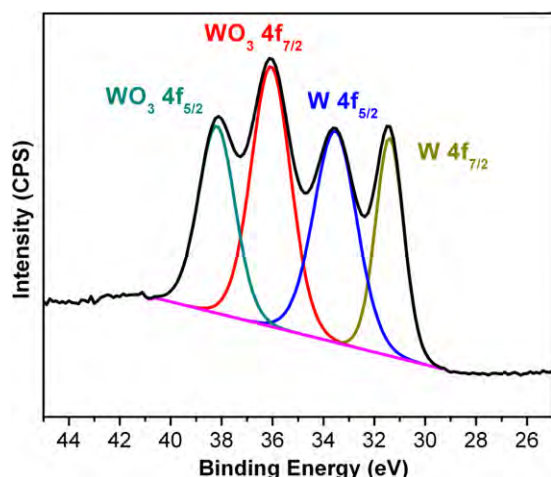


Figure 13. XPS scan of the W 4f peak after 60 AB cycles of W ALD on NO₂/TMA functionalized MWCNTs with 50 AB cycles of Al₂O₃ ALD.

Al, C and O peaks had an average FWHM of ~ 2.5 eV. The typical ratio of Al:O was 2:2.7. The presence of C in the XPS spectrum exceeded the level of expected adventitious C on the surface of the Al₂O₃ film. The extra C content may result from locations where the Al₂O₃ ALD film had cracked on the MWCNTs during sample preparation.

The XPS analysis of the NO₂/TMA functionalized MWCNTs did not detect N. No N was observed for samples before or after argon sputtering. For a monolayer of NO₂ on the MWCNT surface, the expected N signal should be approximately at the XPS detection limit. However, the NO₂ molecules may also desorb from the surface of the MWCNTs. This NO₂ desorption may occur after the Al₂O₃ ALD films crack on the MWCNTs during mechanical agitation in the rotary reactor at 180 °C.

The XPS spectrum of the W/Al₂O₃ bilayers on the MWCNTs is shown in figure 12(d). This spectrum reveals Al, C, O and W and trace quantities of F and Si. F was present at less than 2 at.% and Si was observed in trace amounts at the noise limit. The W 4f_{5/2} and W 4f_{7/2} XPS signals were also examined in more detail at 30–40 eV as displayed in figure 13. The presence of a quadruplet instead of a doublet for W 4f_{5/2} and W 4f_{7/2} indicates the existence of a WO_x film in combination with metallic W.

The WO_x layer on the W ALD film occurs because tungsten metal is not stable in air. When the W/Al₂O₃/MWCNT samples were removed from the rotary reactor and exposed to the atmosphere, a tungsten oxide layer forms on the surface of the W ALD film. After accounting for O bonded to Al, the W:O ratio of 1:3.1 was determined from the WO₃ 4f and O 1s XPS signals. This ratio is consistent with tungsten oxidizing to WO₃. An Al₂O₃ ALD coating on top of the W ALD could serve to passivate the W ALD film and prevent the W film oxidation in the atmosphere.

Models for determining film thickness from XPS analysis rely on smooth, flat samples for accurate measurements [56]. The entangled cluster agglomerates of coated MWCNTs are more like a powder sample. Models can be employed that

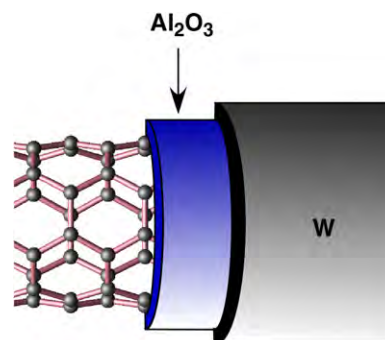


Figure 14. Schematic of coaxial W/Al₂O₃ bilayer on CNT.

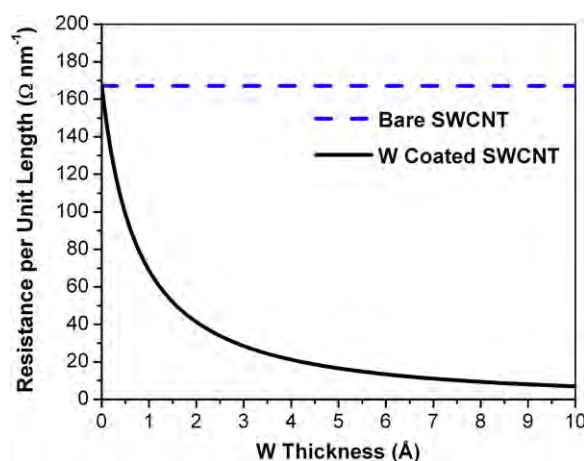


Figure 15. Resistance per unit length for W-coated SWCNT versus W thickness and bare SWCNT.

were developed for analyzing the XPS signals from powder samples. Based on these models [56], the thickness of the WO₃ from XPS measurements is estimated to be ~ 10 – 25 Å. This thickness is close to previously reported values for the thickness of WO₃ on W ALD surfaces [57, 58].

A schematic of a W/Al₂O₃ bilayer on a CNT is shown in figure 14. An additional insulating Al₂O₃ ALD film on this W/Al₂O₃ bilayer would produce a nanocoaxial cable [21]. The CNT is the center conductor, the Al₂O₃ ALD layers are insulators and the W ALD layer is the metallic shield. These nanocoaxial cables may be useful as electrical nanoprobe. Similar nanocoaxial cables have been fabricated by sputtering Al₂O₃ and Cr on vertically aligned MWCNTs and then coating with spin-on glass [59]. The W ALD film thickness in the W/Al₂O₃ bilayer can also be increased to decrease the resistance of a W/Al₂O₃/CNT wire. The W ALD thickness can tune the resistance of the CNT over a wide range.

Using a four-point probe technique, the resistivity of individual single-walled CNTs (SWCNT) was $< 10^{-4} \Omega \text{ cm}$ for nanotubes with a diameter of 13.8 ± 2 Å [60]. From these measurements, the resistance per unit length is $R/L < 167 \Omega \text{ nm}^{-1}$. In comparison, W metal has a resistivity of $5.44 \times 10^{-6} \Omega \text{ cm}$ [61]. Assuming an SWCNT with a diameter of 13.8 Å and $R/L = 167 \Omega \text{ nm}^{-1}$, figure 15 compares the resistance per unit length for a bare SWCNT and a SWCNT coated with various W thicknesses. For the W-coated SWCNT,

the resistance per unit length is progressively reduced versus W thickness. The resistance per unit length is reduced by almost two orders of magnitude with a W thickness of only ~ 10 Å. Note that the calculations did not account for W oxidation or electron scattering at the surface or grain boundaries [62, 63]. Figure 15 serves to illustrate the ability of thin metal films to reduce significantly the resistance of CNTs.

4. Conclusions

Atomic layer deposition (ALD) was performed on quantities of multi-walled carbon nanotubes (MWCNTs) in a rotary reactor. The uncoated and ALD-coated MWCNTs were characterized with transmission electron microscopy and x-ray photoelectron spectroscopy. Al_2O_3 ALD grew as nanospheres on quantities of untreated MWCNTs because of nucleation difficulties. After the NO_2 /TMA nucleation treatment, the Al_2O_3 ALD film grew conformally on the MWCNTs. In addition, the coaxial Al_2O_3 ALD growth on the MWCNTs was approximately linear versus the number of Al_2O_3 ALD reaction cycles.

The Al_2O_3 ALD films were observed to crack on the MWCNTs. More cracking was monitored after crushing and increased mechanical agitation. The coaxial Al_2O_3 ALD films were observed to slide on the surface of the MWCNTs and expose regions of bare MWCNTs. This ease in sliding after cracking of the Al_2O_3 ALD film is consistent with a noncovalently bonded Al_2O_3 ALD film. The Al_2O_3 ALD film also served as a foundation for coaxial W ALD film growth on the MWCNTs. XPS analysis indicated that the W/ Al_2O_3 bilayer on the MWCNTs was covered with a native WO_3 layer. This WO_3 layer results from the exposure of the W ALD film to the atmosphere. The coaxial W ALD film growth on the MWCNTs should significantly reduce the resistance of the W/ Al_2O_3 /MWCNT wire.

Acknowledgments

This research was initially supported by a subcontract from an NSF Phase I SBIR grant to ALD NanoSolutions, Inc. (Broomfield, CO). Subsequent support was provided by the DARPA N/MEMS S&T Fundamentals Program (award no. HR0011-06-1-0048) at the University of Colorado. The authors thank Dr Tom Giddings for his assistance with the TEM. The authors also thank Drs Jarod A McCormick and Arrelaine A Dameron for helpful discussions.

References

- [1] Frank S, Poncharal P, Wang Z L and de Heer W A 1998 *Science* **280** 1744
- [2] Tans S J, Devoret M H, Dai H J, Thess A, Smalley R E, Geerligs L J and Dekker C 1997 *Nature* **386** 474
- [3] Treacy M M J, Ebbesen T W and Gibson J M 1996 *Nature* **381** 678
- [4] Wong E W, Sheehan P E and Lieber C M 1997 *Science* **277** 1971
- [5] Berber S, Kwon Y K and Tomanek D 2000 *Phys. Rev. Lett.* **84** 4613
- [6] Kim P, Shi L, Majumdar A and McEuen P L 2001 *Phys. Rev. Lett.* **87** 215502
- [7] Kong J, Franklin N R, Zhou C W, Chapline M G, Peng S, Cho K J and Dai H J 2000 *Science* **287** 622
- [8] Martel R, Schmidt T, Shea H R, Hertel T and Avouris P 1998 *Appl. Phys. Lett.* **73** 2447
- [9] Deheer W A, Chatelain A and Ugarte D 1995 *Science* **270** 1179
- [10] Dai H J, Hafner J H, Rinzler A G, Colbert D T and Smalley R E 1996 *Nature* **384** 147
- [11] Baughman R H, Zakhidov A A and de Heer W A 2002 *Science* **297** 787
- [12] Thostenson E T, Ren Z F and Chou T W 2001 *Compos. Sci. Technol.* **61** 1899
- [13] George S M, Ott A W and Klaus J W 1996 *J. Phys. Chem.* **100** 13121
- [14] Suntola T 1992 *Thin Solid Films* **216** 84
- [15] Puurunen R L 2005 *J. Appl. Phys.* **97** 52
- [16] Ritala M and Leskela M 2001 Atomic layer deposition *Handbook of Thin Film Materials* (San Diego, CA: Academic)
- [17] Elam J W, Routkevitch D, Mardilovich P P and George S M 2003 *Chem. Mater.* **15** 3507
- [18] Ferguson J D, Weimer A W and George S M 2000 *Thin Solid Films* **371** 95
- [19] Farmer D B and Gordon R G 2005 *Electrochem. Solid-State Lett.* **8** G89
- [20] Farmer D B and Gordon R G 2006 *Nano Lett.* **6** 699
- [21] Herrmann C F, Fabreguette F H, Finch D S, Geiss R and George S M 2005 *Appl. Phys. Lett.* **87** 123110
- [22] Lee J S, Min B, Cho K, Kim S, Park J, Lee Y T, Kim N S, Lee M S, Park S O and Moon J T 2003 *J. Cryst. Growth* **254** 443
- [23] Javey A, Kim H, Brink M, Wang Q, Ural A, Guo J, McIntyre P, McEuen P, Lundstrom M and Dai H J 2002 *Nat. Mater.* **1** 241
- [24] Cao Q, Xia M G, Shim M and Rogers J A 2006 *Adv. Funct. Mater.* **16** 2355
- [25] Green J M, Dong L F, Gutu T, Jiao J, Conley J F and Ono Y 2006 *J. Appl. Phys.* **99** 094308
- [26] Kim D S, Lee S M, Scholz R, Knez M, Goesele U, Fallert J, Kalt H and Zacharias M 2008 *Appl. Phys. Lett.* **93** 103108
- [27] Willinger M G, Neri G, Rauwel E, Bonavita A, Micali G and Pinna N 2008 *Nano Lett.* **8** 4201
- [28] Wank J R, George S M and Weimer A W 2004 *Powder Technol.* **142** 59
- [29] Wank J R, George S M and Weimer A W 2004 *J. Am. Ceram. Soc.* **87** 762
- [30] McCormick J A, Cloutier B L, Weimer A W and George S M 2007 *J. Vac. Sci. Technol. A* **25** 67
- [31] McCormick J A, Rice K P, Paul D F, Weimer A W and George S M 2007 *Chem. Vapor Depos.* **13** 491
- [32] Ramasubramaniam R, Chen J and Liu H Y 2003 *Appl. Phys. Lett.* **83** 2928
- [33] Thostenson E T, Ren Z F and Chou T W 2001 *Compos. Sci. Technol.* **61** 1899
- [34] Coleman J N, Khan U, Blau W J and Gun'ko Y K 2006 *Carbon* **44** 1624
- [35] Lau K T, Gu C and Hui D 2006 *Composites B* **37** 425
- [36] Breuer O and Sundararaj U 2004 *Polym. Compos.* **25** 630
- [37] Tasis D, Tagmatarchis N, Bianco A and Prato M 2006 *Chem. Rev.* **106** 1105
- [38] Bahr J L and Tour J M 2001 *Chem. Mater.* **13** 3823
- [39] Grossiord N, Loos J, Regev O and Koning C E 2006 *Chem. Mater.* **18** 1089
- [40] Lin Y, Taylor S, Li H P, Fernando K A S, Qu L W, Wang W, Gu L R, Zhou B and Sun Y P 2004 *J. Mater. Chem.* **14** 527
- [41] Hernadi K, Fonseca A, Nagy J B, Bernaerts D, Fudala A and Lucas A A 1996 *Zeolites* **17** 416
- [42] Ye Y, Ahn C C, Witham C, Fultz B, Liu J, Rinzler A G, Colbert D, Smith K A and Smalley R E 1999 *Appl. Phys. Lett.* **74** 2307

- [43] Rodriguez N M 1993 *J. Mater. Res.* **8** 3233
- [44] Dillon A C, Ott A W, Way J D and George S M 1995 *Surf. Sci.* **322** 230
- [45] Groner M D, Fabreguette F H, Elam J W and George S M 2004 *Chem. Mater.* **16** 639
- [46] Ott A W, Klaus J W, Johnson J M and George S M 1997 *Thin Solid Films* **292** 135
- [47] Klaus J W, Ferro S J and George S M 2000 *Thin Solid Films* **360** 145
- [48] Grubbs R K, Steinmetz N J and George S M 2004 *J. Vac. Sci. Technol. B* **22** 1811
- [49] Elam J W, Nelson C E, Grubbs R K and George S M 2001 *Surf. Sci.* **479** 121
- [50] Fabreguette F H, Sechrist Z A, Elam J W and George S M 2005 *Thin Solid Films* **488** 103
- [51] Ahn C H, Anczykowski B, Atashbar M Z, Bacsa W, Bainbridge W S, Baldi A, Barnes P D, Batteas J, Bennowitz R and Bhushan B 2007 *Springer Handbook of Nanotechnology* (New York: Springer)
- [52] Grubbs R K, Nelson C E, Steinmetz N J and George S M 2004 *Thin Solid Films* **467** 16
- [53] Sechrist Z A, Fabreguette F H, Heintz O, Phung T M, Johnson D C and George S M 2005 *Chem. Mater.* **17** 3475
- [54] Wind R A, Fabreguette F H, Sechrist Z A and George S M 2009 *J. Appl. Phys.* **105** 074309
- [55] Fabreguette F H, Wind R A and George S M 2006 *Appl. Phys. Lett.* **88** 013116
- [56] Cumpson P J 2000 *Surf. Interface Anal.* **29** 403
- [57] Wilson C A, Goldstein D N, McCormick J A, Weimer A W and George S M 2008 *J. Vac. Sci. Technol. A* **26** 430
- [58] Wilson C A, McCormick J A, Cavanagh A S, Goldstein D N, Weimer A W and George S M 2008 *Thin Solid Films* **516** 6175
- [59] Rybczynski J, Kempa K, Herczynski A, Wang Y, Naughton M J, Ren Z F, Huang Z P, Cai D and Giersig M 2007 *Appl. Phys. Lett.* **90** 021104
- [60] Thess A *et al* 1996 *Science* **273** 483
- [61] Weast R C 1985 *CRC Handbook of Chemistry and Physics* (Boca Raton, FL: CRC Press)
- [62] Rossnagel S M and Kuan T S 2004 *J. Vac. Sci. Technol. B* **22** 240
- [63] Zhang W, Brongersma S H, Richard O, Brijs B, Palmans R, Froyen L and Maex K 2004 *Microelectron. Eng.* **76** 146